Journal of Computers Vol. 35 No. 3, June 2024, pp. 143-158
doi: 10.53106/199115992024063503011

Finite Element Analysis and Simulation Research on Body Welding Hole Shape and Welding Optimization for Automotive Lightweighting

Min-Fei Wen, Lin-Yan Shang*

Tangshan Polytechnic College,
Tangshan City 063299, Hebei Province, China
{wenminfei12345, tgy_linyan}@126.com

Received 13 May 2024; Revised 20 May 2024; Accepted 23 May 2024

Abstract. The lightweight of new energy vehicles is to reduce body weight and process flow while ensuring vehicle safety. The research content of this article is the frame welding process under the integrated die-casting frame technology. Firstly, model different welding shapes, then analyze the fatigue strength of each welding shape and establish a fatigue analysis model; Then, a frame production process model is established, which includes multiple optimization objectives such as production energy consumption, frame stiffness, and load-bearing capacity of welding points. Then, an improved neural algorithm is used to solve the optimal solution of the multi-objective function. Finally, through simulation experiments, the welding shape proposed in this paper can reduce the weight of the vehicle body while ensuring technical indicators. Taking the lightweight of battery enclosure components in the vehicle body structure as an example, an optimized finite element model is obtained, which can ultimately reduce the weight of the optimized battery enclosure components by 3.38 kilograms.

Keywords: lightweight, new energy vehicles, finite element analysis, neural network

1 Introduction

In recent years, with the increase in automobile production and social demand for automobiles, China has quickly entered the ranks of major automobile manufacturing and consumption countries. Conservatively estimated, there are currently about 1.5 billion vehicles worldwide, with a rapid growth rate of 30 million vehicles per year. China alone has about 200 million vehicles [1]. China's automobile production and sales have grown rapidly, and energy consumption cannot be underestimated. Although China is a major energy consuming country, traditional oil resources are relatively scarce. From energy import data, the quantity of imported oil has maintained a very high growth rate, which can be inferred that China's energy consumption and storage problems are relatively serious. Therefore, there is an urgent need to develop new energy vehicles to replace traditional fuel vehicles in the automotive field, thereby improving energy utilization efficiency and reducing dependence on oil resources.

After continuous efforts, China's electric vehicle technology has achieved overtaking on curves, and consumer satisfaction with domestically produced new energy vehicles continues to rise. The willingness to purchase continues to increase, which stimulates the rapid iteration of domestic new energy vehicle technology. In the technology related to electric vehicles, vehicle lightweighting is a key means to enhance the range of electric vehicles. Electric vehicle lightweighting is to reduce the total weight of electric vehicles while ensuring the passive safety, handling stability, riding comfort, NVH performance, and structural strength of the entire vehicle are not affected [2]. The overall structure of a car includes the frame, front and rear hood covers, and doors. As the frame carries most of the weight of the vehicle, it is the most important component of the entire vehicle. Therefore, from the perspective of the overall structure, the structural strength of the frame is highly required. The frame accounts for the largest proportion of the total weight of the vehicle. In automotive lightweighting technology, frame lightweighting is the key point in reducing the total weight of the vehicle and plays a very important role in the lightweighting of the vehicle. The research object of this article is new energy vehicles, therefore, discussing the early lightweight design of new energy vehicles can not only reduce energy consumption in the entire vehicle production process, but also greatly improve the endurance of new energy vehicles and improve the overall power performance of the vehicle.

With the development of automotive lightweight technology and the continuous improvement of integrated

* Corresponding Author

forming technology, researching aluminum alloy car frames with few welding points has become a development direction for various car companies. The overall die-casting of aluminum alloy subframes is difficult, and the general method is to use segmented die-casting and then welding. This poses challenges to the selection of welding methods for casting aluminum alloy subframes, the design of welding joints, the relationship between welding process parameters and forming, mechanical properties, and other welding problems [3].

With the development of integrated molding technology, the integration molding rate of body structural components and covering parts is increasing, which means that there are fewer and fewer welding points, but the welding points have not disappeared. Therefore, this article analyzes and studies the welding forms that occur in the process of integrated molding of car doors. The work done in this article is as follows:

1) Firstly, several common welding shapes were analyzed, and it was found that under the same stress requirements, circular welding holes are the optimal structural design while minimizing the use of welding materials;

2) Based on the manufacturing process of the car body, establish a multivariate optimization model for car body welding, obtain the optimal parameters of the welding process, and use this method to guide the welding process of other structures of the car sound.

3) The ultimate focus of this article is on automobile lightweighting. Based on the final welding process guidance, taking the battery cover in the frame as an example, the weight of the optimized welding process can be calculated through simulation software, achieving a weight reduction of 3.38 kilograms.

Based on the research content of this article, the structure arrangement is as follows:

Chapter 2 is the analysis and comparison of research results by relevant scholars, Chapter 3 is the optimization analysis of welding hole shape, Chapter 4 is the optimization analysis of welding parameters, Chapter 5 is the simulation experiment, which verifies that the weight of the vehicle body is reduced while ensuring mechanical performance. Chapter 6 is the conclusion.

2 Related Work

The significant benefits brought by lightweight technology have led to rapid development, and the application of automotive lightweight technology in the design and development of new car models has also increased significantly. In this regard, major domestic and foreign car companies have accumulated rich technology and experience. With the shortening of the automotive research and development cycle and the gradual maturity of technology, a new car model has fully considered the optimization of automotive performance from the conceptual design stage, and then improved the design of a vehicle model according to market demand and performance requirements. Summarize the process of vehicle lightweighting, mainly focusing on structural optimization and material replacement optimization. In terms of structural optimization, finite element method is mainly used to conduct finite element analysis and simulation of lightweight objects, and the obtained data is used as an important basis for vehicle optimization.

For the research on lightweight technology, foreign car companies have conducted in-depth research on frame lightweight technology for a long time, with Tesla being a typical representative, and its lightweight technology is relatively mature. Tesla cleverly connects computer science, mechanics, and mathematics, and has developed structural finite element analysis and structural optimization techniques based on numerical analysis, leading the way in automotive forming technology.

Tao Chen studied the body of an all aluminum city bus and optimized the roof frame structure based on topology optimization theory. He established a finite element model of the all aluminum bus frame and selected the roof frame with large deformation for topology optimization under two typical working conditions. Based on the topology results, the roof frame was redesigned, and the weight of the frame was reduced. The article used conventional optimization methods, but the optimization speed was slow, and the optimized parameters may not be optimal [4].

Guoli Yun used Nastran software to establish a finite element model of the front subframe of a certain type of electric vehicle. Based on the inertia release theory, the static strength of the subframe was calculated under typical and extreme working conditions. Based on the analysis results, an optimization design scheme was proposed to change the thickness of the swing arm mounting bracket to 2.5mm and increase the weld seam area at the left and right installation points of the steering gear. The overall design met the performance requirements of the frame and optimized the weight of the frame. However, in the article, the frame thickness was changed to 2.5mm mainly through empirical methods, which were obtained through intelligent solving algorithms [5].

In 2010, Professor Yuanfang Fu and others from Tsinghua University studied the frame structure of small elec-

tric vehicles and constructed a simple model for topology optimization of this small car, implementing topology optimization. Firstly, reliability analysis and design work were conducted, followed by a detailed analysis of the topology optimization results. A structure with high energy absorption efficiency was constructed, and the reliability of the optimization results was verified. This study can not only reduce the weight of the frame structure, but also ensure the safety of the vehicle model [6].

In 2015, Zonghui Lai used sensitivity analysis to divide the bus skeleton into blocks, which reduced the dimensions of the design variables for optimizing the size of the bus skeleton. He used a combination of multi-objective optimization and size optimization to design the lightweight of the bus skeleton. With all safety performance indicators of the bus meeting national standards, the skeleton weight was ultimately reduced by 460kg. This modular grouping optimization idea provides a theoretical reference for size optimization of complex structures of household electric cars [7].

The above analysis provides reference significance for achieving the parameter optimization goal of automotive manufacturing technology by analyzing the relevant methods of automotive lightweighting from early to modern at home and abroad. However, the above research results do not provide an optimization process for the specific structure of automobiles.

In terms of selecting welding holes, welding methods, and welding strength analysis for vehicle welding, domestic and foreign scholars have also conducted multiple studies. This article summarizes and analyzes the research results of some domestic and foreign scholars. This article summarizes and analyzes the research results of some scholars at home and abroad. Fuquan Wang separately cut the material at the weld seam, used laser marking method to record the deformation and displacement of the laser marked grid in the tensile test through a real-time microscopic recording system, and calculated the stress-strain curve of the material. The results showed that the highest true stress in the weld seam was larger than that of the substrate, and the Young's modulus, initial yield stress, and strength coefficient of the weld seam were greater than those of the substrate, while the strain hardening index was smaller than that of the substrate [8].

Ping Wu studied ST12 and 304 steel welded plates using nanoindentation method and found that the elastic-plastic mechanical properties of the substrate were very different from those of the weld seam and heat affected zone metal of the welded plate. The Young's modulus, initial yield stress, and strength coefficient of the substrate were smaller than the values of the heat affected zone metal, while the strain hardening index was larger than the values of the heat affected zone metal. The elastic-plastic mechanical properties of weld metal and heat affected zone metal are also different [9].

After summary and analysis, although vehicle lightweighting reduces welding, welding still exists. Different welding base materials and welding processes may lead to different welding effects. Therefore, this article aims to study the impact of welding methods on vehicle frames.

3 Analysis of Welding Hole Shape and Welding Method

Different manufacturers and models of vehicles use different welding methods during the frame welding process. Different welding methods and hole shapes determine the quality and stiffness of the frame, which are the two most basic parameters in the current lightweight process of automobiles. Therefore, this article starts with the shape of the welding hole, analyzes the finite element model and fatigue strength model of different welding hole shapes, and analyzes the impact of different shapes of welding holes and different welding methods on the quality and stiffness of the frame.

3.1 Welding Hole Shape Design

In order to demonstrate the performance of the designed welding hole shape in this article, three different welding hole shapes of welding samples were designed for comparison. The welding hole designs were circular, runway shaped, and square. Drawing on the design principles of ablation experiments, in order to highlight the influence of shape on welding performance, the effective welding area of the three different welding hole samples, i.e. the projection area of the weld metal on the non welding hole plate, remained the same. In the finite element model of circular welded hole specimens, the welded plate and weld metal were simulated using 8-node Solid45 solid elements, with a total of 7397 elements and 10722 nodes. The material properties of the weld metal and the base metal are the same, with a density of $7950 kg / m^3$, an elastic modulus of $193 GPa$, and a Poisson's ratio of

0.3. The load is uniformly applied to the nodes in the width direction of the welded plate, with a size of 5*KN* and a direction parallel to the length direction of the plate. The node at the load end of the pad plate is constrained to move in the *y* and *z* directions, while the other end is constrained to move in the *x*, *y* and *z* directions. In the finite element model of the runway shaped welded hole specimen, there are a total of 10056 elements and 14748 nodes; In the finite element model of the square welded hole specimen, there are a total of 7927 elements and 12543 nodes, and the material properties, element types, loads, and constraints are exactly the same as those of the circular welded hole specimen [10].

The size of the designed weld hole specimen is shown in Fig. 1, and the shape of the designed weld hole is shown in Fig. 2. The other two specimens have the same size as the circular weld hole specimen except for the weld hole.

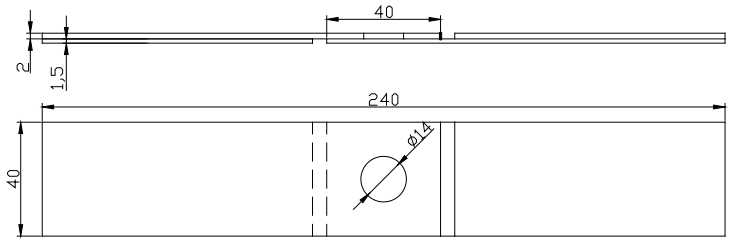

Fig. 1. Size and structure of welded hole specimens

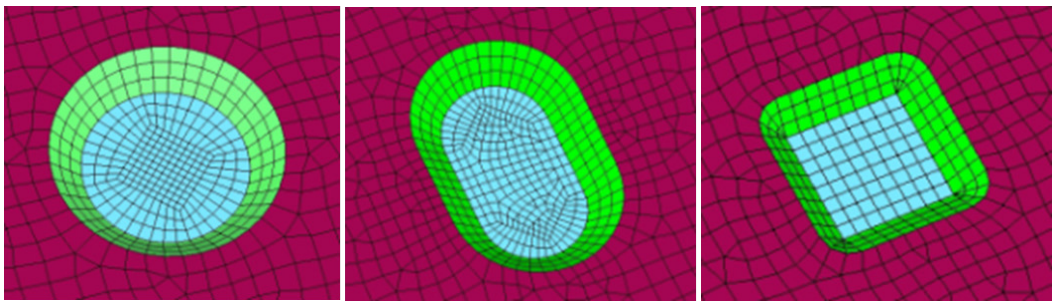

Fig. 2. Weld hole shape

Conduct strength analysis on three types of specimens separately, and observe the magnitude and distribution of stress at the solder joints of the specimens. Fig. 3, Fig. 4, and Fig. 5 show the stress cloud maps of the bonding surfaces of two plates with circular, runway, and square welded hole specimens subjected to loads, respectively.

From the results of finite element analysis, it can be seen that the maximum stress of the circular welded hole specimen welded hole plate and non welded hole plate both occur in the arc-shaped area at the junction of the two plates and the weld metal near the stress end, at 310*MPa* and 377*MPa*, respectively. The maximum stress of the runway shaped welded hole specimen welded hole plate and non welded hole plate both occur at the transition between the arc-shaped and straight parts at the junction of the inner surface of the two plates and the weld metal near the stress end, at 334*MPa* and 381*MPa*, respectively. The maximum stress of the square welded hole specimen welded hole plate and non welded hole plate both occur at the corner of the junction of the inner surface of the two plates and the weld metal near the stress end, respectively. 319*MPa* and 417*MPa*. Under the same load and effective welding area, the maximum stress at the internal bonding surface of the two plates of the circular welded hole specimen is the smallest, and the stress concentration coefficient is relatively small compared to the other two types of welded hole specimens. Therefore, from the results of strength analysis, it is better to choose circular welded holes for frame welding [11].

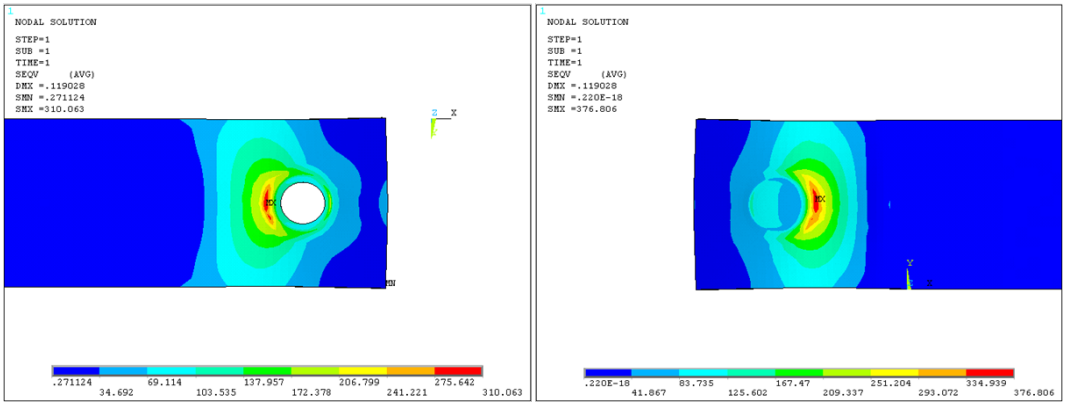

Fig. 3. Stress cloud map of the bonding surface between two circular welded hole specimens

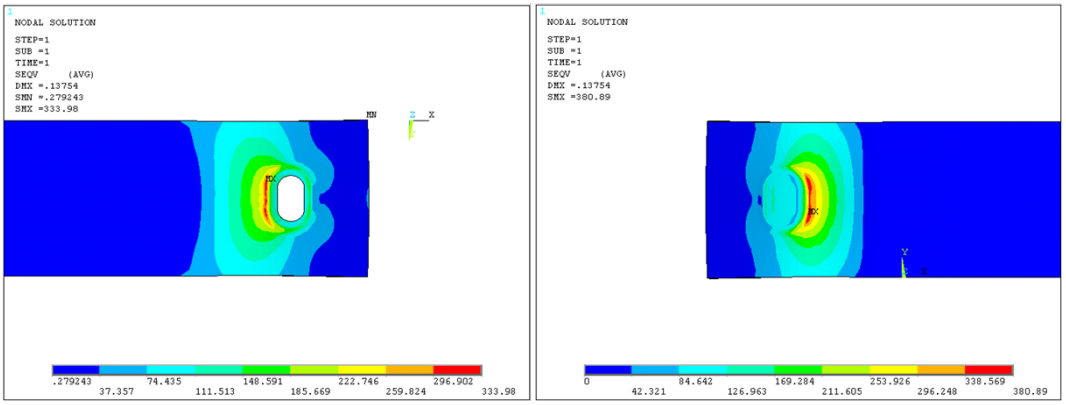

Fig. 4. Stress cloud map of the bonding surface between two plates of a runway shaped welded hole specimen

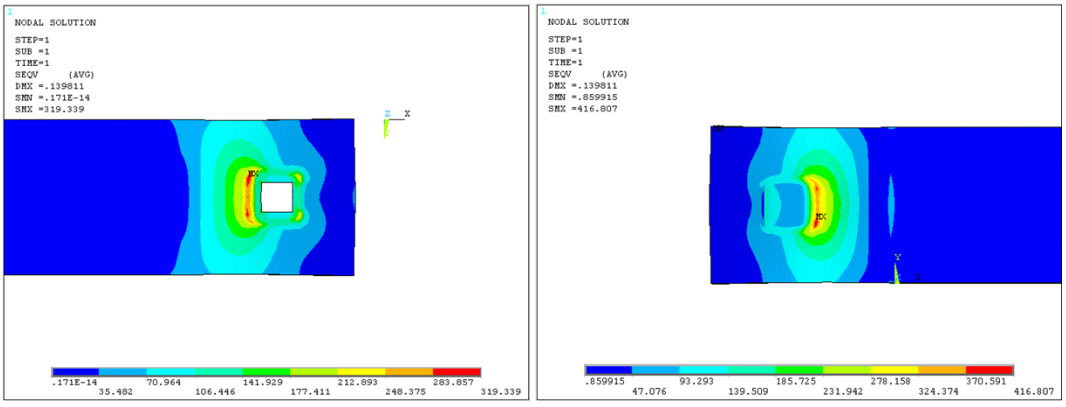

Fig. 5. Stress cloud map of the bonding surface between two square welded hole specimens

3.2 Fatigue Strength Analysis of Circular Welding Hole Ring Welding

Using an elastic shell element shell63 with 3 translational node degrees of freedom and 3 rotational node degrees of freedom with thin film and bending effects to simulate a weld nugget, and connecting the upper and lower

plates. The time required to establish this model is short, the model is simple, and the quality constraint effect on the element mesh of the metal plate is not significant. The thickness of the inclined shell element is equal to the maximum plate thickness of 4*mm*. At the same time, the shell element around the weld core is thickened to simulate the stiffness of the weld seam. The thickness of the shell element here is equal to the sum of the thicknesses of the two plates divided by $\sqrt[3]{2}$. The calculation is as follows:

$$t = \frac{t_1 + t_2}{\sqrt[3]{2}} = 0.7937\left(t_1 + t_2\right) = 4.7622mm \ . \tag{1}$$

Set the shell units in this area to a thickness of 4*mm*. The specific structure is shown in Fig. 6. The model consists of 1899 units and 1962 nodes.

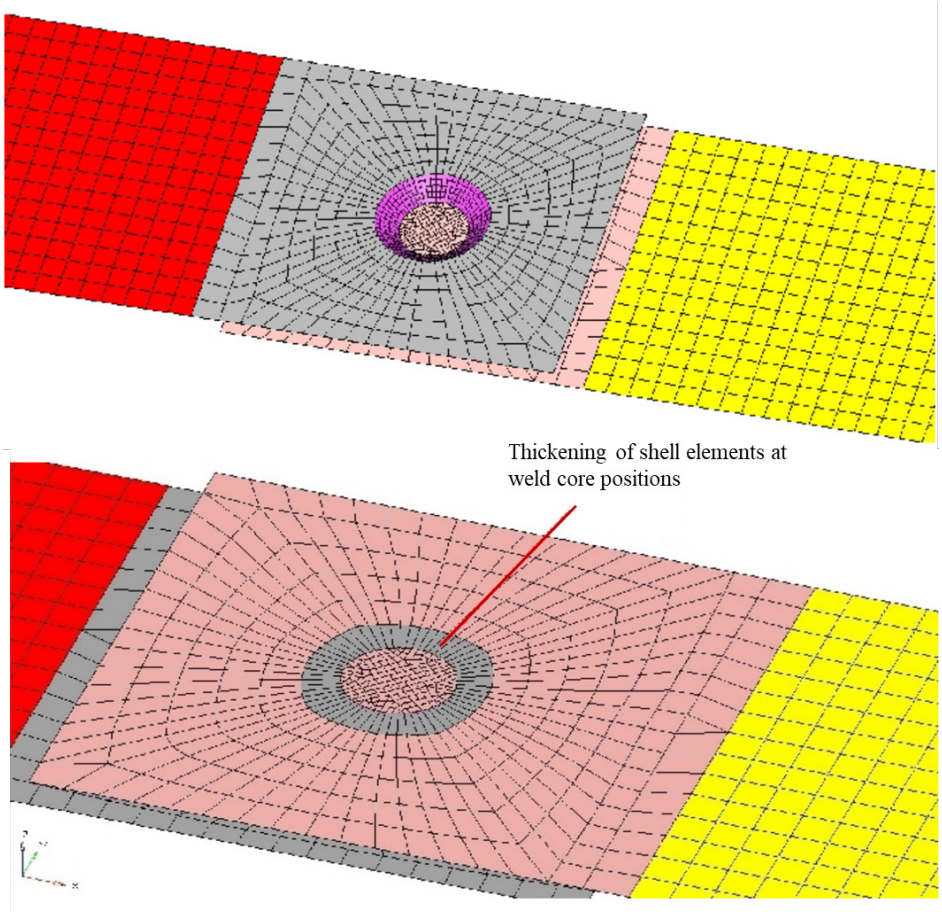

Fig. 6. Shell unit welding hole model

After the above analysis, an analytical model for the welding shape of the welding object was established.

3.3 Fatigue Experiment and Result Analysis of Ring Welding Process

Firstly, set up an experimental testing environment, and the welding process fatigue strength analysis process is shown in Fig. 7.

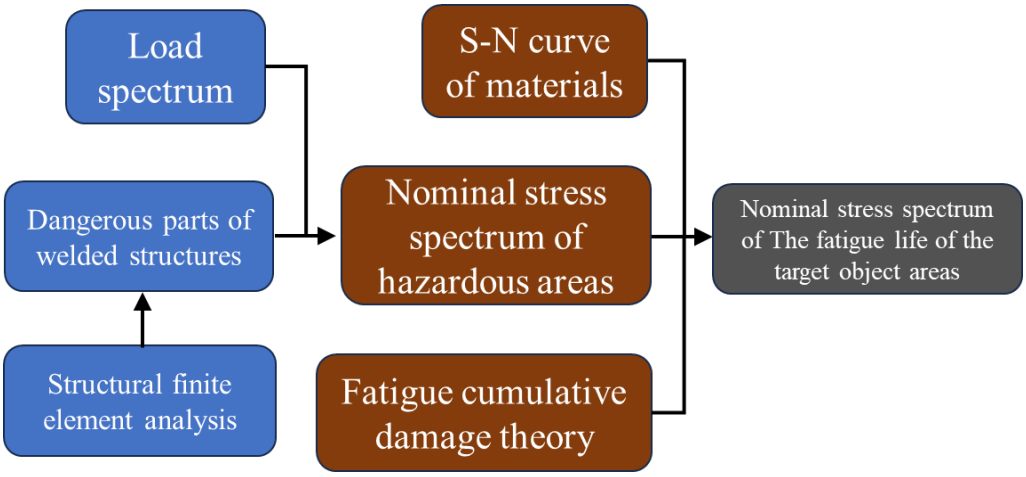

Fig. 7. Schematic diagram of fatigue strength analysis process

1) Determine the hazardous areas of welded components based on stress analysis and measured results, or experience.

2) Convert the fatigue load spectrum obtained through specifications or measurements into the stress spectrum of the nominal stress of the hazardous area using mathematical statistical methods.

3) Establish a linear relationship curve ($S-N$ curve) between the logarithmic fatigue life (N) of the component and the logarithmic stress level (S), or use the $S-N$ curve of the material to establish an approximate $S-N$ curve of the component.

4) Applying linear fatigue cumulative damage theory for fatigue life estimation. The use of nominal stress method to evaluate fatigue life can cause significant errors, mainly due to the fact that the $S-N$ curve provided is the median curve of fatigue test data, which has the property of statistical averaging. Moreover, this evaluation method ignores residual stresses caused by plastic deformation during fatigue loading. But based on good engineering judgment and providing relatively accurate raw data, a conservative design can be obtained [12].

The fatigue test was conducted on a $10kN$ high-frequency fatigue testing machine with a stress ratio of $R = 0.1$. From a mechanical perspective, the two welded plates connected by the solder joint can transmit tensile/shear forces and torsional moments. As the load increases, the solder joint undergoes plastic deformation in both tensile and shear directions. When the plastic deformation exceeds the failure strain, fatigue fracture occurs at the solder joint, leading to failure. The median load-life curve of the component was obtained through experiments, and the curve is described as follows:

$$\log P = -0.26301 * \log N + 2.162 \quad . \tag{2}$$

Due to the fact that the $S-N$ curves of most existing materials are measured under certain specifications, processing techniques, and specified loading conditions, but due to the complexity of boundary conditions and geometric uncertainty of components in practical situations, using the existing material $S-N$ curves directly as the $S-N$ curves of the entire component or structure is not consistent with reality when applied. Therefore, this article will modify the $S-N$ curve of the material based on the data obtained from the experiment. The materials used in the component are as mentioned earlier. In order to calculate the fatigue life of the component under different simulation methods, in the absence of actual material $S-N$ parameters, the load-life curve obtained through experiments was selected to approximate the $S-N$ parameters of the two materials used in the component, as shown in Table 1.

Generate the $S-N$ curve of the component material according to the material parameters listed in Table 1, as shown in Fig. 8.

Table 1. S-N parameters of materials

	SUS301L-MT	SUS301L-HT
SRI1	4133.7MPa	4173.0MPa
b_1	-0.26301	-0.26301
*NC*1	1E7	1E7
b_2	0	0
RR	0.1	0.1
YS	480MPa	685MPa
UTS	820MPa	930MPa

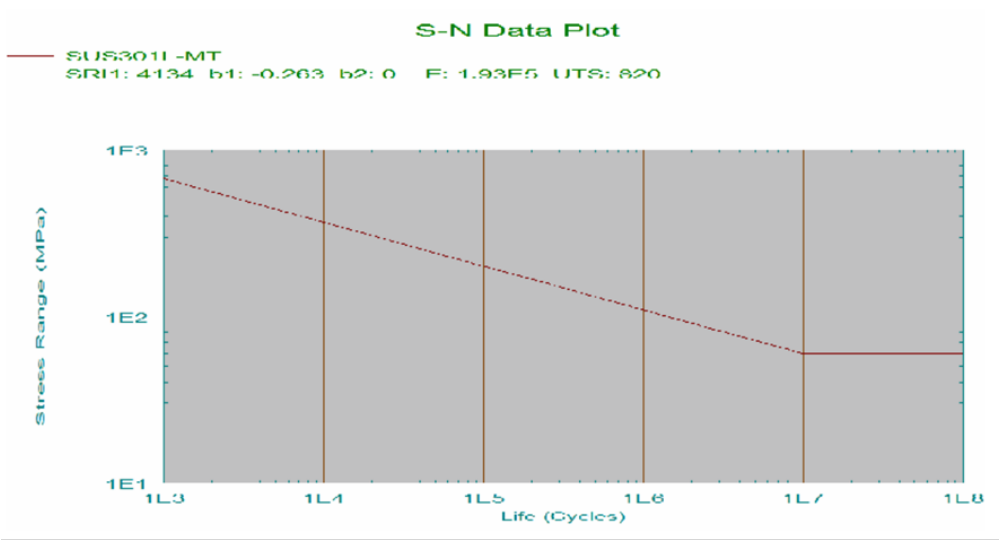

(a) S-N curve of SUS301L-MT

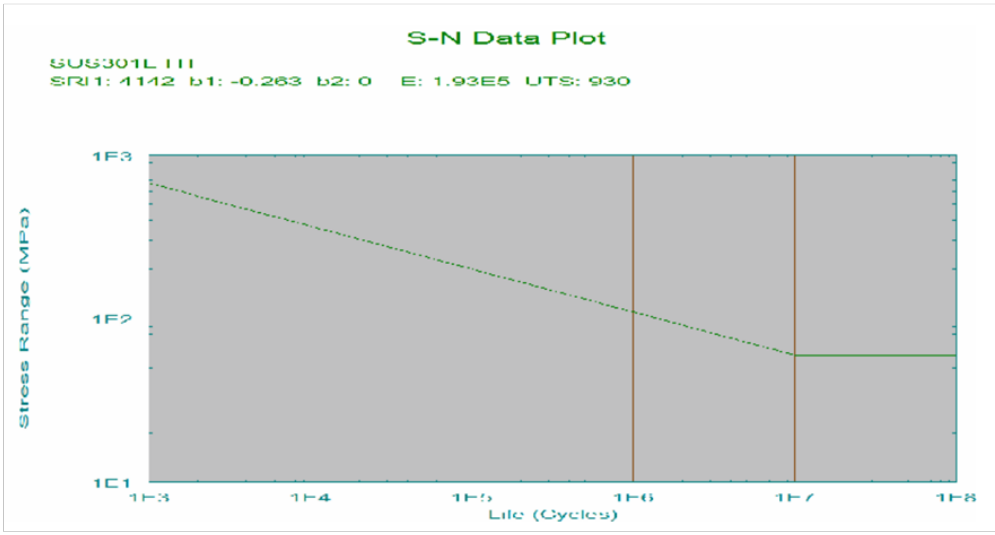

(b) S-N curve of SUS301L-HT

Fig. 8. S-N curve

The setting of the load spectrum is shown in Fig. 9, using a constant amplitude load spectrum with $R = 0.1$, a frequency of $0.5Hz$, and a load amplitude of $10kN$.

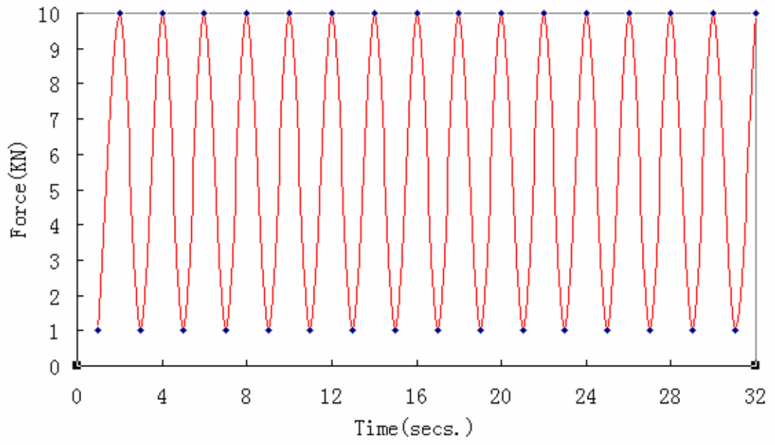

Fig. 9. Fatigue load spectrum

After the above analysis, the model settings have been completed, providing a basic condition for parameter optimization.

4 Optimization of Frame Welding Parameters

After the above analysis, various factors such as welding method, weld joint shape, and welding temperature have a significant impact on the fatigue strength of welded parts. The influence of various parameters on welding is mutually restrictive, that is, how to allocate reasonable weights to each welding condition during the welding process is the purpose of this section. This article uses neural network algorithms to design and achieve the optimal combination of welding parameters under different welding requirements.

4.1 Solder Joint Load

The most basic requirement for welding points is to ensure the mechanical performance requirements of the vehicle body. A good welding point must first meet the basic mechanical performance of the welding point under the comprehensive load of the vehicle body, and at the same time, seek to minimize the processing energy consumption of the welding process. The modeling of the welding point load and energy consumption is as follows:

$$\begin{cases} \min & Q \\ s.t. & F_c > F_s \end{cases}. \tag{3}$$

In the formula, A represents the energy consumption during the welding process, B represents the load-bearing capacity of the solder joint, and C represents the force magnitude of the solder joint under the comprehensive working conditions of the vehicle body. By considering the stress on the solder joints in the vehicle's working conditions and the low energy consumption during the welding process, the obtained solder joints not only meet the requirements in terms of solder joint morphology, but also truly meet the mechanical performance requirements of the vehicle's solder joints, while also achieving energy conservation and low-carbon. Therefore, the new standard for evaluating the quality of solder joints is more applicable to current product design concepts and development guidelines [13].

Welding production is an important energy consumption link in vehicle production. In welding production, in addition to normal tooling and equipment costs, electrical energy consumption and electrode head loss are also important cost factors. The wear of electrodes is directly related to the strength of welding parameter specifications. Therefore, the energy loss determined by welding current and welding time is the focus of this article and the optimization objective of the mathematical model. The expression for welding heat is:

$$Q = \int_0^T I^2 \left(r_c + 2r_{ew} + 2r_w \right) d_t \quad . \tag{4}$$

In the formula, I is the welding current, r_c is the contact resistance between the workpiece, r_{ew} is the contact resistance between the electrode and the workpiece, r_w is the internal resistance of the workpiece, and t is the welding time.

4.2 Welding Optimization Model Expression

In the process of frame production, quality and cost are often a pair of contradictory and unified contradictions. When excessively pursuing manufacturing quality, it will inevitably lead to excessive production costs; When excessively pursuing production costs, it can lead to issues with product quality and quantity reliability. How to obtain more reasonable quality and control production costs remains the optimization goal of this article. Therefore, this article establishes a function optimization model that includes quality control weights and cost control weights.

Let $X = (x_1, x_2, \ldots, x_n)$ be the input variable of dimension n, and y be the output variable Assuming there are m sample points $(x_1, x_2, \ldots, x_m)$, the function relationship $y_i = y\ (X_i)(i = 1, 2, \ldots, m)$ between the output variable and the input variable is the response approximation function. Considering both fitting accuracy and fitting efficiency, the response surface modeling method based on radial basis functions is most suitable for practical problems. The radial basis function expression is as follows:

$$y = y(X) = \sum_{i=1}^{P} \lambda_i^{'} f_i^{'}(X) + \sum_{j=1}^{m} \delta_i \theta\left(\left\| X - X^i \right\| \right) . \tag{5}$$

In the formula, $f^{'}(X) = \{f_1(X), f_2(X), \ldots, f_p(X)\}$ is the regression function, $\lambda_i^{'}$ is the regression function of $f^{'}(X)$, $\theta(X)$ is the basis function, and $||X - X^{'}||$ is the Euclidean norm.

Welding points are an important guarantee for ensuring the mechanical properties of the vehicle body. Therefore, it is necessary to first meet the basic mechanical properties of the welding points under the comprehensive working conditions of the vehicle body. Secondly, due to the limitation of welding production rhythm, there are requirements for welding time. Excessive welding time will reduce production rhythm and affect production efficiency; Short welding time makes it difficult to ensure the quality of the solder joints. In addition, considering the control of welding spatter, it is required that the welding current should not be too high. Therefore, under the aforementioned engineering constraints, in order to balance the relationship between solder joint quality and welding energy consumption, and obtain optimal welding parameters. The optimization model is as follows:

$$\begin{cases} \min & Q \\ & TS_c > F_j \\ s.t. & CT_c > F_l \\ & T_{\max} > t > T_{\min} \end{cases} . \tag{6}$$

In the formula, Q represents welding energy consumption, TS_c and CT_c respectively represent the shear and tensile strength of the welded joint obtained under a certain welding parameter combination, F_j and F_l respectively represent the shear and tensile strength of the welded joint under the comprehensive working conditions of the vehicle body, $T_{\max}$ and $T_{\min}$ respectively represent the maximum and minimum welding time allowed during the welding process.

4.3 Using Neural Networks to Solve the Optimal Welding Parameters

The model construction of BP neural network mainly consists of input layer, hidden layer, and output layer. The number of neurons in the input layer of a neural network is generally the same as the number of input signals. In this paper, the input signals include welding time, welding current, welding cost, and welding energy consumption. Therefore, the number of neurons in the input layer is determined to be 4. The number of neurons in the output layer is generally the same as the number of indicators of the output signal. This article takes the shear strength of solder joints as the output indicator, so the number of neurons in the output layer is determined to be 1. The number of hidden layer nodes is represented as:

$$n = \sqrt{n_a + n_b} + k \ . \tag{7}$$

Table n represents the number of hidden layer nodes, n_a represents the number of input layer nodes, n_b represents the number of output layer nodes, and k represents any integer between 1 and 10. Therefore, after calculation, the number of hidden layers is between 4-12.

Select the experience value of the welding machine as the existing data sample, call the random selection command to allocate 10 sets of training samples and 6 sets of testing samples, select the learning rate value of 0.01, and set it to dynamically adjustable, with a target error of 0.001 and a momentum factor of 0.8. Choose *mse* as the performance function, select different numbers of hidden layer neurons to train the neural network, set the number of hidden layer neurons to 9, and simulate in Matlab. The convergence curve of the neural network model is shown in Fig. 10.

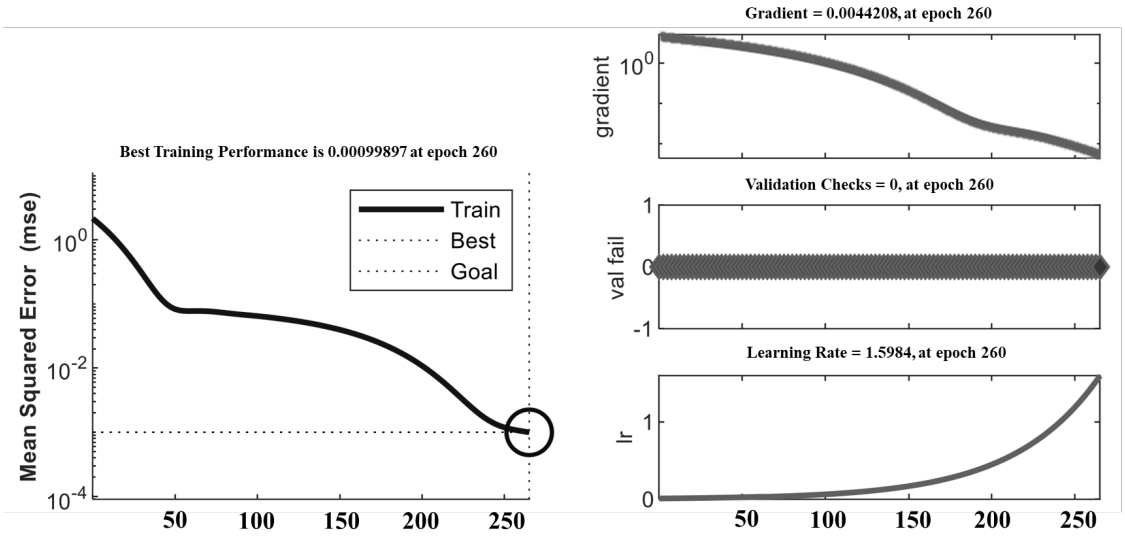

Fig. 10. Fatigue load spectrum

When establishing a prediction model for welding parameter optimization through BP neural network, the distribution of network weights and thresholds has a significant impact on the performance of the network. The weights of the network are initially randomly generated between [0, 1], and during the training process of the BP neural network, they are gradually adjusted based on the backpropagation characteristics of the neural network, resulting in a better weight distribution [14]. The network prediction process is shown in Fig. 11.

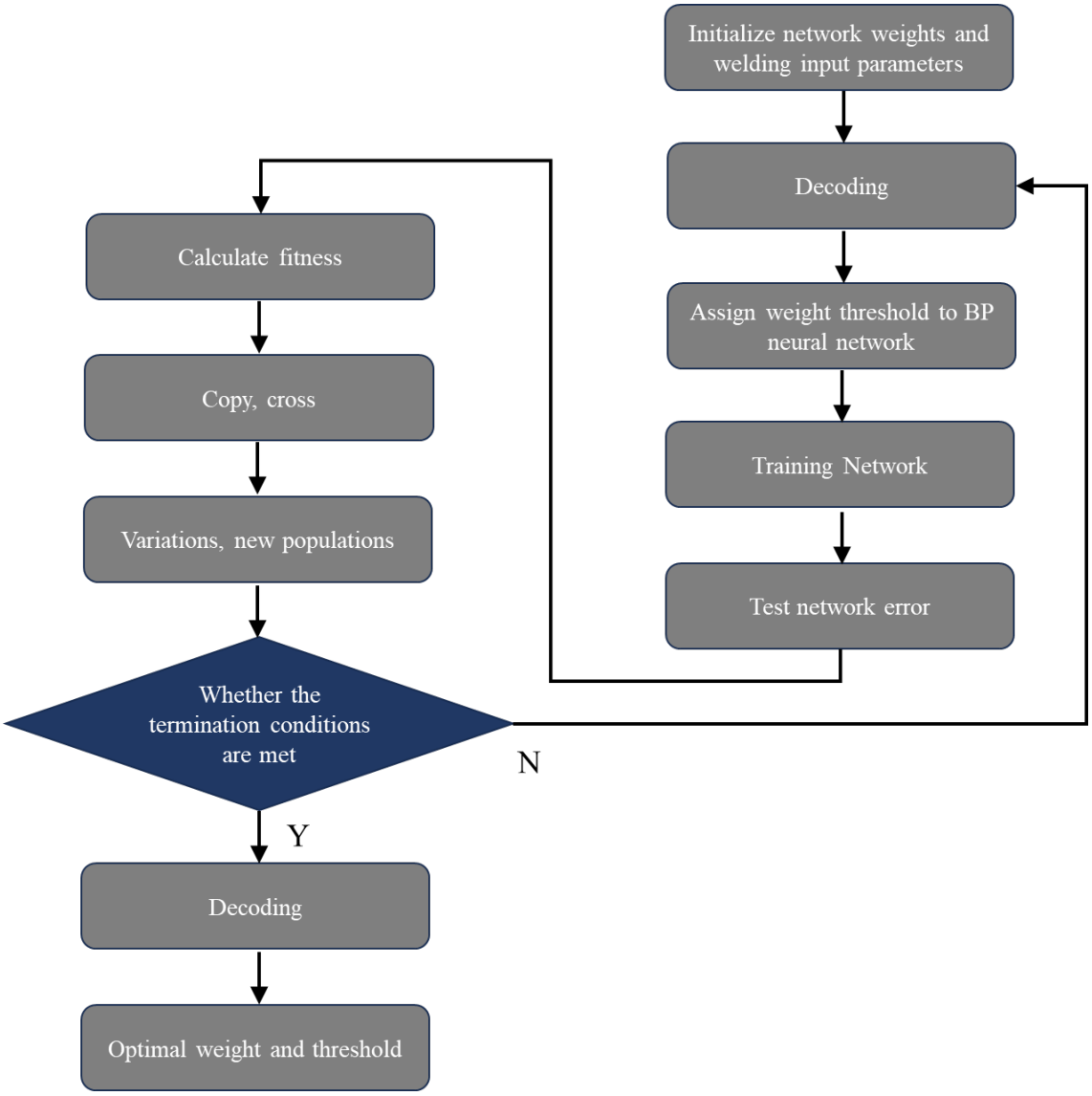

Fig. 11. Prediction process

The pseudocode for the search process is as follows in Table 2:

Table 2. Model solving steps

Algorithm. Solution steps
1: Input: Training Set
2: Initial weight and initial value;
3: data normalization;
4: Create a network
5: while True do
6: Forward propagation
7: Backpropagation
8: Using the network
9: data normalization
10: end while
11: Output: Complete training and output optimized values

After the above analysis, an optimization model for welding was established. In order to seek the final welding process parameters, this paper used a neural network algorithm and established an optimization flowchart for the algorithm.

5 Welding Parameter Optimization Simulation and Result Analysis

Based on the neural network model constructed earlier, the process parameters were optimized by selecting a welding power range of [55%, 85%], a welding time range of [50*ms*, 80*ms*], a shielding gas pressure range of [600*MPa*, 1200*MPa*], and a welding height range of [0.9*mm*, 1.2*mm*]. 8000 values were randomly selected for each process parameter in their respective intervals, forming a total of 8000 sets of process parameter combinations. Then, the previously trained network model was used for prediction, and the prediction results are shown in Table 3.

Table 3. Prediction results

Welding action time	Nitrogen pressure	Welding height	Obtain strength
68ms	1037Pa	1mm	59.31Mpa

By inputting optimal instructions in Matlab and targeting welding quality and energy consumption, the optimal process parameters were obtained: welding action time of 68*ms*, protective gas nitrogen pressure of 1037*Pa*, welding height of 1*mm*, and corresponding strength of 59.31*MPa*. In the previous section 3.3, the optimal process parameters were also inferred through orthogonal experiments, and the optimal combination was obtained as welding action time of 70*ms*, nitrogen pressure of 1000*MPa*, and welding height of 1*mm*, it was found that the optimal combination of the two parameters resulted in a welding height of 1*mm* for both.

To further verify the feasibility of the optimal welding results, analyze the fatigue strength of the welded joint after using this welding parameter. This section adopts a constant amplitude load spectrum with $R = 0.1$, with a frequency of 05*Hz* and a load amplitude of 10*kN*. The process of change over time is shown in Fig. 6

Different finite element simulation models based on ring welding were imported into NCode software, and the fatigue life of corresponding components under tensile shear fatigue loads was calculated for five typical simulation methods. The influence of different simulation methods on the fatigue performance of the structure was investigated. Using the nominal stress method, the fatigue life of components under the same working condition was calculated for five simulation methods, and the stress of dangerous parts obtained through static analysis was also included in the Table 4.

Table 4. Prediction results

Finite element model	Fatigue life	Error value	Fatigue damage value	Static analysis results	Failure location
Welding point model at a certain point on the frame	30374	3.08%	$4.135e^{-5}$	348.8	Near the weld nugget

After the above analysis, the corresponding fatigue life cloud map is shown in Fig. 12.

From the static analysis stress cloud map and fatigue life cloud map of the finite element model of the above ring welding structure, it can be seen that the dangerous parts of the structure obtained through static analysis and fatigue analysis are consistent, and the fatigue failure of these models occurs near the weld core.

After using the new welding process, with the same welding process requirements, a lighter and less energy consuming welding method can be used. Therefore, the adopted welding point structure and the designed vehicle body will be imported into SolidWorks for analysis, and a finite element model will be established to obtain the improved structural weight. Taking the battery cladding component in the vehicle body structure as an example, the battery weight obtained by improving the welding method and die casting method is shown in Table 5, and the cladding component structure is shown in Fig. 13.

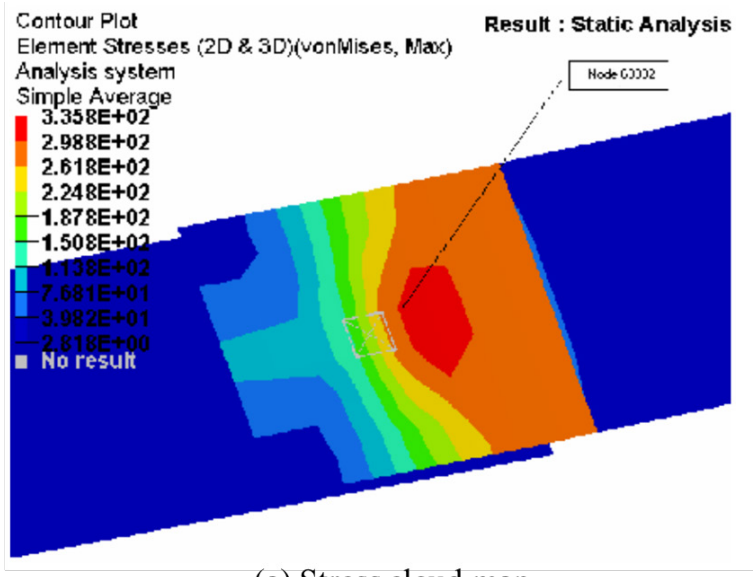

(a) Stress cloud map

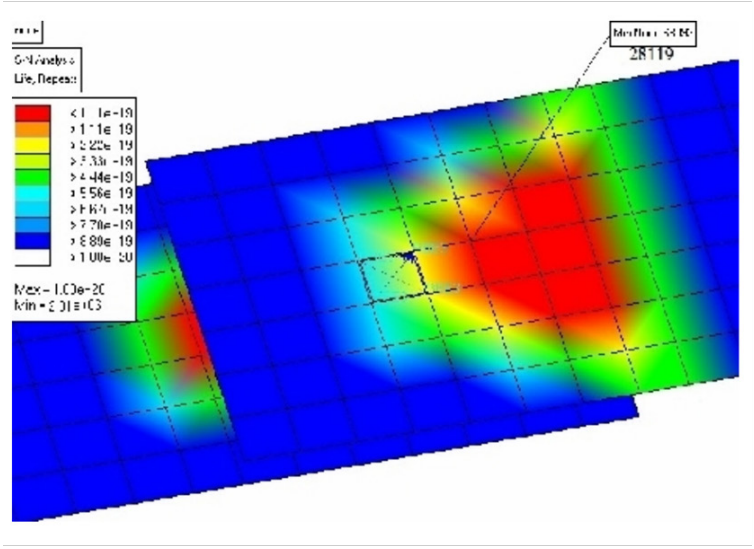

(b) Fatigue life cloud map

Fig. 12. Stress and lifespan cloud map of the model

Table 5. Prediction results

Variable name	Value before optimization	Optimized value	Weight reduction value
Side panel thickness	3.5mm	2.016mm	1.23Kg
Support 1 thickness	2.9mm	1.980mm	1.03Kg
Support 2 thickness	2.7mm	2.002mm	0.74Kg
Support 3 thickness	2.8mm	1.973mm	0.38Kg

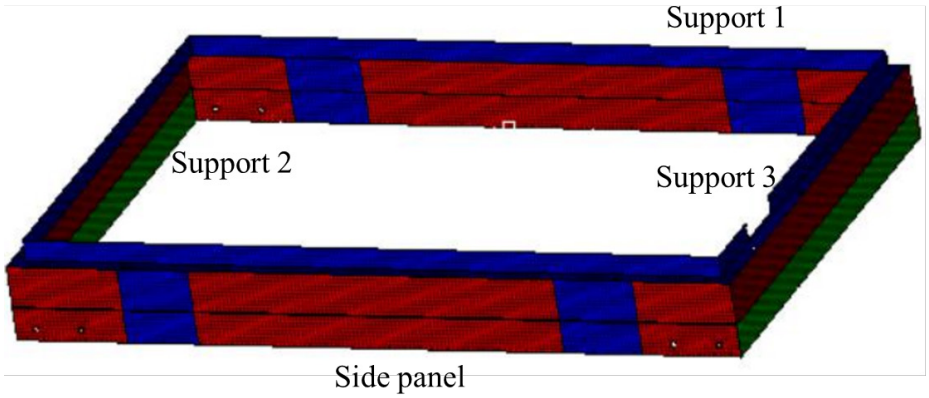

Fig. 13. Optimized bracket structure

After the analysis in this section, the optimal welding structure of the vehicle body can be obtained, and the weight of the vehicle body can be reduced by 13.41%. At the same time, the methods proposed in this article provide reference for the design of other body structures and white body.

6 Conclusion

Automobile lightweighting and integrated die-casting are the current development directions in structural design and manufacturing of new energy vehicles. This article takes a small amount of welding after automobile die-casting as the research object. Firstly, several common welding shapes are analyzed, and it is concluded that under the same stress requirements, circular welding holes are the optimal structural design while minimizing welding materials. Then, based on the manufacturing process of the car body, a multivariate optimization model for car body welding is established to obtain the optimal parameters of the welding process, and this method is used to guide the welding process of other structures of the car sound. Finally, the ultimate focus of this article is on automobile lightweighting. Based on the final welding process guidance, taking the battery cover in the frame as an example, the weight of the optimized welding process can be calculated through simulation software, achieving a weight reduction of 3.38 kilograms.

References

[1] S.-Y. Zhang, C. Gao, Y.-P. Gong, J.-H. Lv, G.-J. Wang, Research on the Development Status and Strategy of New Energy Vehicles under the Background of “Carbon Neutrality”, Auto Time (21)(2023) 89-91.
[2] B. Zhang, L.-F. Shi, X.-H. Jin, Design and Application of a Digital-Driven Simulation Optimization System for Lightweight Entire Vehicle Structure, System Simulation Technology 19(4)(2023) 334-338.
[3] X.-Z. Li, Integrated Die Casting Technologies of Aluminum Alloy, Automobile Technology & Material (7)(2023) 17-21.
[4] T. Chen, F. He, X.-S. Jiang, Y. Zhou, Lightweight Design of Roof Frame of Pure Electric Bus, J Agricultural Equipment & Vehicle Engineering 60(10)(2022) 52-55+108.
[5] G.-L. Yun, X.-J. Xi, J.-W. Zhao, H. Luan, P.-P. Zhi, Analysis and Optimization of Electric Vehicle Frame Strength Based on Simulation Analysis, Mechanical Engineer (8)(2023) 119-122.
[6] Y.-F. Fu, D.-F. Jin, W.-W. Qiao, Topological Optimization design on the body structure of minielectric cars under multi-working conditions, Journal of Machine Design 27(2)(2010) 77-80.
[7] Z.-H. Lai, L.-Q. Gu, Y. Zhang, The Structural Analysis and Optimal Design of A Pure Electric Bus Body Structure, Drive System Technique 31(4)(2017) 35-39.
[8] F.-Q. Wang, S.-H. Wang, G.-Q. Li, M.-F. Ding, Research on the Application of Plasma Welding Technology in Sealing Welding of Railway Vehicle, Materials Protection 55(6)(2022) 182-185.

[9] P. Wu, X. Lan, X.-H. Wang, X.-L. Liu, G.-F. Xie, Research on loading curve of BGA solder balls by nanoindentation, Electronic Components and Materials 40(12)(2021) 1221-1227.
[10] M.-F. Wen, L.-T. Lu, Optimization analysis of different hole shapes on ring-weld structures of SUS301L corrosion resistant plate, Machinery 39(6)(2012) 1-3+10.
[11] Q. Liu, B.-B. Tian, F. Zhao, Numerical Simulation of Plate Welding Thermal Structural Coupling Field Based on ANSYS, Mechanical Engineer (8)(2023) 30-33.
[12] J.-B. Zhang, Z. Hu, J.-L. Zhang, C. Wang, T.-G. Zou, Review of Advances in Fatigue S-N Curve Prediction Models, Science Technology and Engineering 23(13)(2023) 5390-5411.
[13] C. Gao, C.-Y. Huang, Y. Liang, S.-F. Liu, H.-Q. Zhang, Stress analysis and optimization of POP stacked solder joints under thermal cyclic load, Transactions of the China Welding Institution 44(2)(2023) 74-82+133-134.
[14] X.-P. Gao, F. Chen, Y.-S. Wang, X. Huang, G.-Q. Tong, Optimization of Micro Resistance Spot Welding Process Parameters Based on Genetic Algorithm and Neural Network, Aerospace Materials & Technology 48(3)(2018) 33-37.